Chinese Journal of
POLYMER SCIENCE

RESEARCH ARTICLE

https://doi.org/10.1007/s10118-026-3869-1
Chinese J. Polym. Sci.

Cyano-functionalized Halogenated Benzene Additives for Efficient and Stable Organic Solar Cells

Yang-Yang Zhang†, Xiang-Lun Xie†, Xin-Kang Wang, Kai-Yuan Lv, Tong-Jia Liu, Lian-Jie Zhang*, and Jun-Wu Chen*

Institute of Polymer Optoelectronic Materials and Devices, Guangdong Basic Research Center of Excellence for Energy and Information Polymer Materials, State Key Laboratory of Luminescent Materials and Devices, South China University of Technology, Guangzhou 510640, China

Electronic Supplementary Information

Abstract Volatile solid additives based on halogenated benzenes have recently emerged as pivotal components for optimizing the morphology of bulk-heterojunction (BHJ) active layers in organic solar cells (OSCs). However, the generally weak electron-withdrawing nature of halogen substituents results in restricted non-covalent interactions with the electron-deficient moieties of the acceptor. Herein, we propose a novel additive strategy involving the introduction of a non-halogenated, strongly electron-withdrawing cyano group to the benzene ring. Three cyano-functionalized halogenated benzene additives 3,5-difluorobenzonitrile (DFNB), 3,5-dichlorobenzonitrile (DCNB), and 3,5-dibromobenzonitrile (DBNB) are designed for the first time to modulate the morphology of blend films, thereby enhancing the efficiency and stability of OSCs. In contrast to the additive-free films, the additive-processed BHJ films exhibit well-defined fibrillar network structures. The introduction of these additives effectively suppressed bimolecular recombination while promoting exciton dissociation and charge transport, leading to significantly improved photovoltaic performance of the OSCs. As a result, the DCNB-processed PM6:L8-BO devices achieved a remarkable power conversion efficiency (PCE) of 19.05% versus 17.24% of the control, while also showing superior ambient storage stability, retaining 87% of the initial PCE after 1900 h, versus 75% for the control devices. This study provides a simple strategy based on cyano-functionalized halogenated benzene additives to optimize the morphology and thus improve the efficiency and stability of OSCs.

Keywords Organic solar cells; Cyano-functionalized halogenated benzenes; Volatile solid additives; Morphology optimization

Citation: Zhang, Y. Y.; Xie, X. L.; Wang, X. K.; Lv, K. Y.; Liu, T. J.; Zhang, L. J.; Chen, J. W. Cyano-functionalized halogenated benzene additives for efficient and stable organic solar cells. *Chinese J. Polym. Sci.* https://doi.org/10.1007/s10118-026-3869-1

INTRODUCTION

Organic solar cells (OSCs) have garnered significant attention in the field of green energy conversion owing to their light weight, mechanical flexibility, solution processability, and semitransparency.[1–5] With the continuous development of novel conjugated polymer donors (D) and non-fullerene acceptors (A), the power conversion efficiencies (PCEs) of single-junction OSCs have exceeded 20%.[6–9] The morphology of the active layer plays a pivotal role in governing exciton dissociation and charge transport, ultimately determining the PCE of OSCs.[10,11] An ideal bulk-heterojunction (BHJ) morphology should feature both sufficient D/A interfaces and adequate phase separation.[12] Specifically, the domain size should be within the exciton diffusion length (10–20 nm) to ensure efficient exciton dissociation, whereas an interconnected bicontinuous network is required to facilitate charge transport to the electrodes.[11,13–16] However, the inherent conflict between the film formation kinetics and thermodynamics during spin-coating frequently impedes the realization of optimal nanoscale phase separation and bicontinuous morphology, inevitably leading to trap-assisted recombination and energy loss.[17,18] Therefore, numerous strategies have been proposed for optimizing the morphology of the active layer to enhance the photovoltaic performance of OSCs, including thermal annealing,[19,20] ternary composition strategies,[21–23] and additive engineering.[24–26] Additive engineering has been widely employed owing to its ease of post-processing, low cost, and effectiveness.[6,27–29]

Recently, volatile solid additives based on halogenated benzenes have emerged as a promising strategy for optimizing the morphology of active layers in OSCs. Song *et al*. introduced an asymmetric volatile solid additive, 1,3-dibromo-5-chlorobenzene (DBCl), which was coupled with the dithienothiophene[3,2-*b*]pyrrolobenzothiadiazole (BTP) core unit of a Y-series acceptor. This interaction induces an anisotropic dipole orientation, elevates the dipole moment, and establishes distinct interlayer non-covalent interactions, thereby promoting more compact molecular packing and en-

* Corresponding authors, E-mail: lianjiezhang@scut.edu.cn (L.J.Z.)
E-mail: psjwchen@scut.edu.cn (J.W.C.)
† These authors contributed equally to this work.
Invited Research Article
Received June 30, 2026; Accepted August 28, 2026; Published online October 26, 2026

© Chinese Chemical Society
Institute of Chemistry, Chinese Academy of Sciences

hanced crystallinity. This synergistic effect suppressed trap-assisted recombination, facilitated exciton dissociation and charge transport, and ultimately enabled the PM6:L8-BO-based device to deliver a high PCE of 18.50% with an outstanding fill factor (FF) of 80.20%.[30] The Hou group employed low-cost, highly volatile 3,5-dichlorobromobenzene (DCBB) as a solid additive to optimize the BHJ morphology of PBQx-TF:eC9-2Cl blend films. The incorporation of DCBB modulated the aggregation behavior of PBQx-TF and eC9-2Cl during film formation, inducing favorable phase separation and reinforced molecular packing, which afforded a remarkable PCE of 19.20%, the highest reported for binary OSCs at that time.[31]

We are interested in developing additives with fast removal properties that can be easily removed from the active layer.[32–35] In this study, we introduce three low-cost, highly volatile solid additives, 3,5-difluorobenzonitrile (DFNB), 3,5-dichlorobenzonitrile (DCNB), and 3,5-dibromobenzonitrile (DBNB), for the first time. Owing to the strong electron-withdrawing nature of the cyano (—CN) group, these additives are expected to reinforce intermolecular interactions with the donor and acceptor components, thereby enabling favorable morphology regulation and ultimately enhancing the performance and stability of OSCs. Systematic simulations revealed the electrostatic potential (ESP) distributions of the three additives and their non-covalent interactions with the donor and acceptor components. The additives DFNB, DCNB, and DBNB exhibit larger dipole moments (2.85, 2.98, and 3.01 Debye, respectively) than conventional halogenated benzene additives, and the enhanced polarity strengthens their non-covalent interactions with both PM6 and L8-BO.[30,31] All three additives preferentially interacted with the benzodithiophene (BDT) unit of PM6 and the BTP unit of L8-BO, with DCNB and DBNB exhibiting notably higher binding energies (ΔE_b) and stronger intermolecular interactions than DFNB. The additive-processed BHJ films exhibited well-defined fibrillar network structures, in contrast to the additive-free films. The introduction of these additives effectively suppressed bimolecular recombination while promoting exciton dissociation and charge transport, leading to significantly improved photovoltaic performance of the OSCs. As a result, the DCNB-processed PM6:L8-BO-based device achieved a remarkable PCE of 19.05%, compared to 17.24% for the control device, driven by the enhanced short-circuit current density (J_{SC}) and FF. Moreover, the DCNB-processed devices exhibited superior stability, retaining 87% of the initial PCE after 1900 h compared versus 75% for the control devices. This study provides a simple strategy based on cyano-functionalized halogenated benzene additives to optimize the morphology and thus improve the efficiency and stability of OSCs and elucidate the underlying mechanism.

EXPERIMENTAL

The device fabrication methods and related testing and characterization techniques are presented in the electronic supplementary information (ESI).

RESULTS AND DISCUSSION

The molecular structures of donor PM6, acceptor L8-BO, and three additives (DFNB, DCNB, and DBNB) are illustrated in Figs. 1(a) and 1(b). Thermogravimetric analysis (TGA) was conducted to investigate the thermal properties of the additives. As shown in Figs. S1(a)–S1(c) (in ESI), the decomposition temperatures (T_d, 5% weight loss) for DFNB, DCNB, and DBNB are of 63, 110, and 139 °C, respectively, while the corresponding complete sublimation temperatures are of 113, 173, and 215 °C. Furthermore, the volatility of these additives was studied by spin-coating a highly concentrated chloroform solution onto Si wafers. As presented in Fig. S1(d) (in ESI), DFNB was fully removed during the spin-coating of its chloroform solution, confirming its in situ removability[33] as a solid additive. For conventional trihalogenated benzene solid additives,[30,31,36] complete volatilization was typically achieved by thermal annealing at 75–90 °C for 1–12 min (Table S1 in ESI), whereas our cyano-functionalized additives, DCNB and DBNB, completely volatilized at 90 °C within only 1 and 5 s, respectively (Figs. S1e and S1f in ESI).

To verify the interactions between the three additives and active layer materials, density functional theory (DFT) was employed to calculate the ESP distributions of DFNB, DCNB, and DBNB. Computational details regarding the structural optimization, wave-function analysis, and visualization tools are provided in ESI. The strong electron-withdrawing nature of the cyano (—CN) group creates distinct charge separation within the additive molecule. As depicted in Fig. S2 (in ESI), the —CN group in all three additives exhibited a negative potential distribution, whereas the benzene ring frameworks displayed positive potential distributions. In addition, compared with conventional halogenated benzene additives (0.19 Debye for DBCl[30], and 2.26 Debye for DCBB[31]), additives DFNB, DCNB, and DBNB exhibit substantially larger dipole moments of 2.85, 2.98, and 3.01 Debye, respectively, consistent with the increasing polarizability of the halogen atoms (F < Cl < Br). These pronounced and well-oriented dipoles enabled the non-covalent association of the cyano-functionalized additives with the polarized segments of PM6 and L8-BO, thereby modulating the aggregation behavior of both the donor and acceptor. In a previous report, polymer PM6 had a negative potential dominated distribution throughout the main chain, whereas acceptor L8-BO showed an almost positive potential distribution along the backbone.[37] Afterward, the semi-empirical xTB method[38] was employed to simulate the optimal geometric configurations and calculate the corresponding ΔE_b of the three additives with PM6 and L8-BO. Figs. 1(c) and 1(d) show that all three additives preferentially interacted with the BDT unit of PM6 and the BTP core unit of L8-BO. The calculated ΔE_b values of DFNB, DCNB, and DBNB with the BDT unit of PM6 were −17.28, −17.63, and −21.96 kcal·mol^{-1}, respectively, suggesting that DCNB and DBNB exhibit stronger intermolecular interactions with PM6 than DFNB. The ΔE_b values between the BTP core unit of L8-BO and the additives DCNB and DBNB were −18.69 and −20.07 kcal·mol^{-1}, respectively, significantly higher than that of DFNB (−15.02 kcal·mol^{-1}), indicating that DCNB and DBNB interact more strongly with L8-BO.

The effects of the three additives on the molecular aggregation behavior of the neat and blended films were further investigated using UV-Vis absorption spectra. The corresponding absorption spectra are shown in Figs. 2(a)–2(c), and

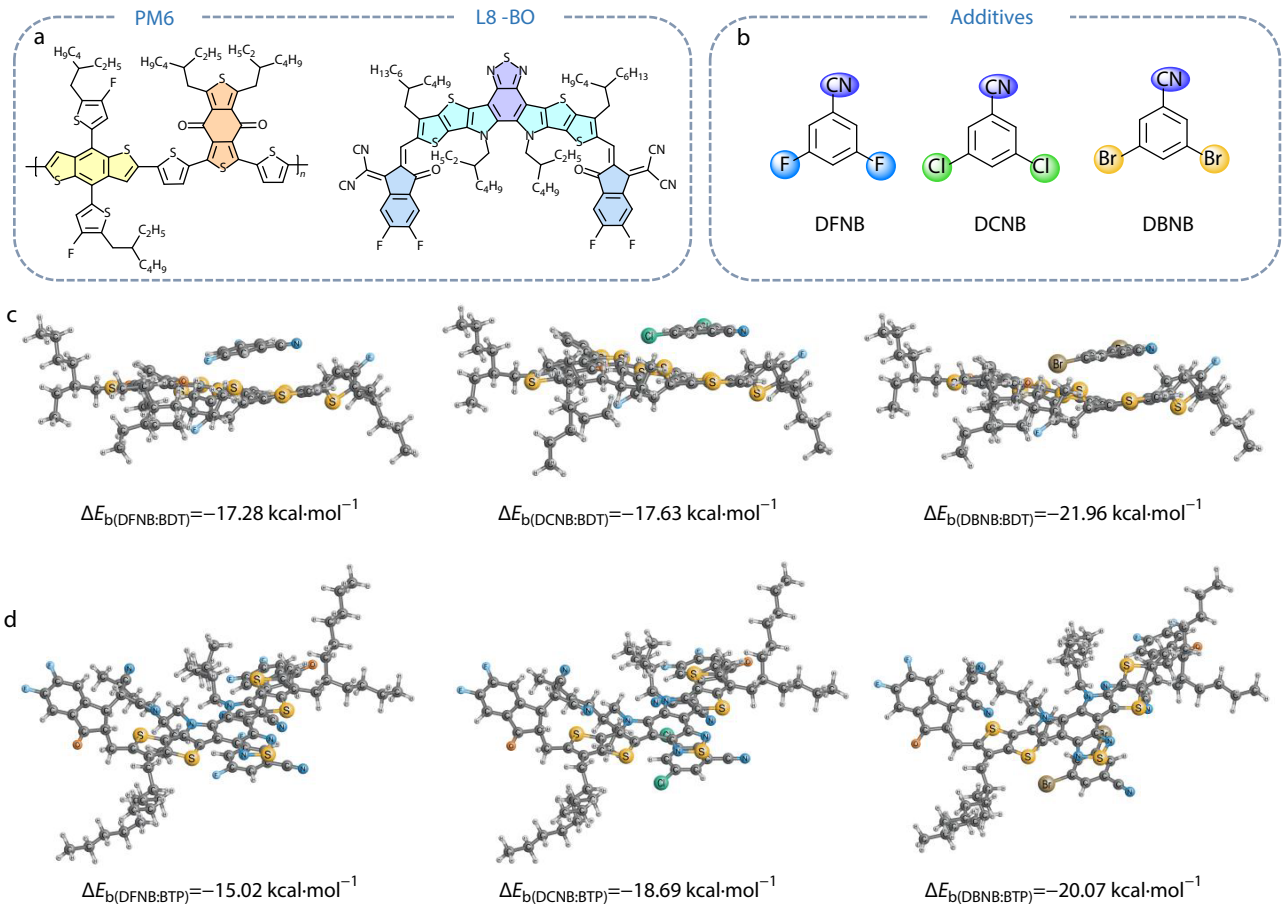


Fig. 1 (a) Molecular structures of PM6 and L8-BO; (b) Chemical structures of the additives DFNB, DCNB, and DBNB; The optimized geometry modeled and corresponding binding energy (ΔE_b) for complex clusters of (c) additive:BDT of PM6 and (d) additive:BTP of L8-BO.

the related partially zoomed spectra are shown in Figs. S3(a)–S3(c) (in ESI). Compared with the as-cast and DFNB-treated PM6 films, the DCNB- and DBNB-treated films exhibited increased $I_{0\text{-}0}/I_{0\text{-}1}$ ratios for the 0-0 and 0-1 absorption peaks, from 1.076 to 1.081 and 1.092, respectively (Table S2 in ESI). A similar trend was observed for the L8-BO neat films, where the $I_{0\text{-}0}/I_{0\text{-}1}$ ratios were significantly enhanced upon treatment with the DCNB and DBNB additives. Moreover, the incorporation of DCNB and DBNB induced slight red-shifts in the 0-0 absorption peaks for both the PM6 and L8-BO neat films. The results indicate that the additives DCNB and DBNB exhibit stronger intermolecular interactions with both the donor and acceptor, in agreement with the binding energies obtained from our DFT calculations. For the PM6:L8-BO blend films, significantly increased absorption coefficients of PM6 were observed, while the maximum absorption peak and the absorption edge of L8-BO all exhibited slight red-shifting. The results suggest enhanced molecular aggregation of both the polymer donor and non-fullerene acceptor in the presence of DCNB and DBNB.[6,39]

To evaluate the additive effect on photovoltaic performance, OSCs with the conventional device architecture of ITO/PEDOT:PSS/PM6:L8-BO/PDINN/Ag were fabricated. First, the additive content was optimized. As the additive concentration increased, the FF progressively improved at the expense of the open-circuit voltage (V_{OC}), with an optimal concentration of 4.5 mg·mL^{-1} identified for all three additives (Tables S3–S5 in ESI). The photovoltaic parameters of the optimized devices, including J_{SC}, V_{OC}, FF, and PCE, are summarized in Table 1, and the corresponding current density-voltage (*J-V*) curves are shown in Fig. 2(d). For the control device without an additive, a PCE of 17.24% was achieved, based on a V_{OC} of 0.895 V, J_{SC} of 25.74 mA·cm^{-2}, and FF of 74.85%. When processed with DFNB, the PCE increased to 18.26%, with improved J_{SC} and FF, but a slightly decreased V_{OC}. For the DBNB-treated device, the PCE further increased to 18.68%, along with a higher FF of 79.13%. Notably, the device fabricated with DCNB achieved a champion PCE of 19.05%, accompanied by an enhanced J_{SC} of 27.20 mA·cm^{-2} and an impressive FF of 79.29%. External quantum efficiency (EQE) spectra of the devices are shown in Fig. 2(e). The integrated J_{cal} values from the EQE spectra are summarized in Table 1 and show excellent agreement with the corresponding J_{SC} values from the *J-V* curves, demonstrating the reliability of the photovoltaic performance. The efficiency-distributed box plots of the PCEs derived from 10 independent devices per system are presented in Fig. S4 (in ESI). The DFNB-, DCNB-, and DBNB-processed OSCs exhibited average PCEs of 18.11%, 18.96%, and 18.60%, respectively, which were remarkably higher than that of 17.13% for the control. The statistical PCE results confirm the substantial photovoltaic performance enhancement achieved with cyanobenzene-based

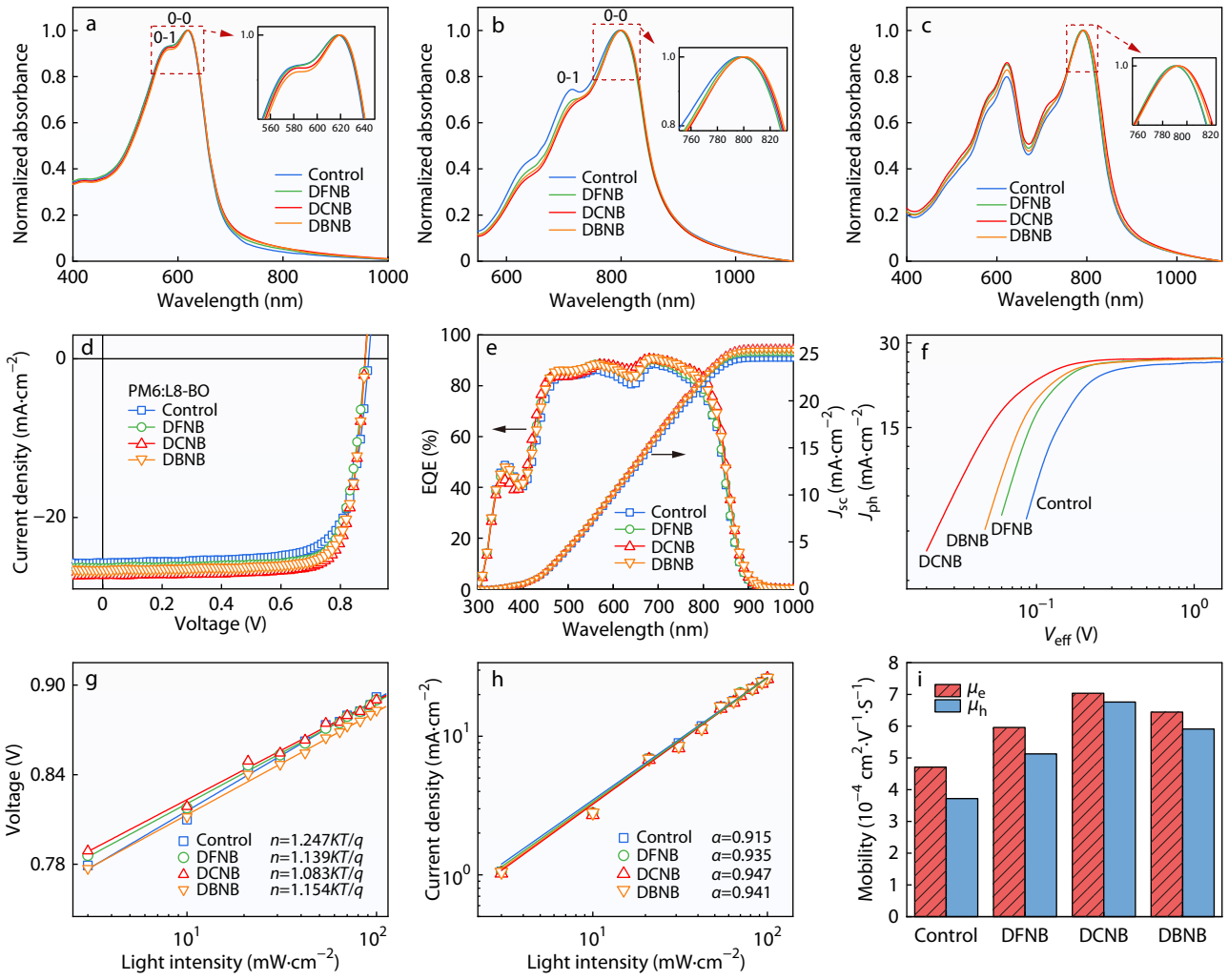


Fig. 2 Normalized UV-Vis absorption spectra of (a) PM6 neat films, (b) L8-BO neat films, and (c) PM6:L8-BO blend films with or without additives; (d) *J*-*V* and (e) EQE curves of the optimized PM6:L8-BO-based OSCs with or without additives; (f) The J_{ph}-V_{eff} curves; (g) The V_{OC}-P_{light} curves; (h) The J_{SC}-P_{light} curves; (i) Electron and hole mobilities of the PM6:L8-BO-based OSCs with or without additives.

Table 1 Photovoltaic parameters of the optimized PM6:L8-BO-based OSCs processed with different additives.

PM6:L8-BO	V_{OC} (V)	J_{SC} (mA·cm^{-2})	FF (%)	PCE [a] (%)	J_{cal} [b] (mA·cm^{-2})
Control	0.895 (0.890±0.002)	25.74 (25.84±0.130)	74.85 (74.54±0.402)	17.24 (17.18±0.075)	24.45
DFNB	0.884 (0.880±0.005)	26.37 (26.28±0.212)	78.35 (78.43±0.615)	18.26 (18.18±0.062)	25.07
DCNB	0.883 (0.880±0.002)	27.20 (27.22±0.247)	79.29 (78.80±0.445)	19.05 (18.97±0.056)	25.69
DBNB	0.884 (0.880±0.002)	26.69 (26.73±0.214)	79.13 (78.82±0.511)	18.68 (18.58±0.075)	25.37

[a] The average values based on 10 devices are given in parentheses; [b] Integrated from EQE curves.

additives. This improvement is primarily attributed to the concurrent increase in J_{SC} and FF, suggesting that modulating molecular aggregation *via* DFNB, DCNB, and DBNB additives is an effective strategy.

The photovoltaic performance of OSCs is closely associated with exciton dissociation and charge recombination dynamics. The photocurrent density versus effective voltage (J_{ph}-V_{eff}) curves were employed to evaluate the effects of the additives on the exciton dissociation probability (P_{diss}) and charge collection efficiency (P_{coll}), as shown in Fig. 2(f). P_{diss} and P_{coll} can be obtained from the equations $P_{diss} = J_{ph}^*/J_{sat}$ and $P_{coll} = J_{max}/J_{sat}$, respectively.[34,40] Here, $J_{ph} = J_L - J_D$, where J_L and J_D are the current densities under illumination and dark conditions, respectively. V_{eff} is defined as $V_{eff} = V_0 - V$, where V_0 is the voltage when J_{ph} equals zero, and V is the applied voltage. Generally, J_{sat} is taken as the J_{ph} at V_{eff}=1.5 V, whereas J_{ph}^* and J_{max} denote J_{ph} under short-circuit and maximum power output, respectively. As shown in Table S6 (in ESI), the DFNB-, DCNB-, and DBNB-processed OSCs displayed P_{diss} values of 92.58%, 95.90%, and 93.50% and P_{coll} values of 91.35%, 93.36%, and 92.51%, respectively, which outperformed the control device (88.81% for P_{diss} and 88.07% for P_{coll}). All the additive-processed devices exhibited enhanced exciton dissociation and charge collection relative to the control, with DCNB showing the most pronounced improvement, consistent with its higher J_{SC} and FF. To gain a deeper understand-

ing of the charge recombination dynamics, we further explored the V_{OC}-P_{light} and J_{SC}-P_{light} relationships (Figs. 2g and 2h), where P_{light} denotes the light intensity. The dependence of V_{OC} on P_{light} is described as $V_{OC} \propto nk_BTq^{-1}\ln(P_{light})$.[41] Here, k_B, T, and q refer to the Boltzmann constant, temperature in Kelvin, and elementary charge, respectively. The ideality factor n determines the type of recombination, with n close to 1 as a bimolecular recombination-dominated case and n close to 2 as a trap-assisted recombination-dominated case.[42] As shown in Fig. 2(g), relative to the control device, the introduction of DFNB, DCNB, and DBNB reduced the ideality factor n from 1.247 to 1.139, 1.083, and 1.154, respectively, indicating suppressed trap-assisted recombination. Additionally, the correlation between J_{SC} and P_{light} follows the equation $J_{SC} \propto P_{light}^{\alpha}$, which α is used to evaluate the strength of the bimolecular recombination.[43] As shown in Fig. 2(h), all three additives increased α compared to the control (0.915), with DCNB affording the highest value closest to 1 (0.947), suggesting that bimolecular recombination was effectively suppressed. Furthermore, the electron mobility (μ_e) and hole mobility (μ_h) of the OSCs processed with different additives were measured using the space charge limited current (SCLC) method (Fig. 2i).[44] The $J^{1/2}$-V curves and relevant parameters are shown in Fig. S5 and Table S7 (in ESI). The control film shows μ_e of 4.71×10^{-4} $cm^2\cdot V^{-1}\cdot s^{-1}$ and μ_h of 3.72×10^{-4} $cm^2\cdot V^{-1}\cdot s^{-1}$, giving a μ_e/μ_h ratio of 1.27. Compared with the control device, the three additive-treated devices exhibited enhanced μ_e and μ_h, leading to a more balanced charge transport with μ_e/μ_h ratios ranging from 1.09 to 1.16. Impressively, the DCNB-treated device delivered the highest μ_e (7.04×10^{-4} $cm^2\cdot V^{-1}\cdot s^{-1}$) and μ_h (6.76×10^{-4} $cm^2\cdot V^{-1}\cdot s^{-1}$), affording more balanced transport with a μ_e/μ_h ratio of 1.04. The higher and more balanced charge transport characteristics partially explain why the DCNB-treated device achieved the highest J_{SC} and FF values.

To investigate the microscopic morphology of the PM6:L8-BO blend films, atomic force microscopy (AFM) and transmission electron microscopy (TEM) were used to investigate. As depicted in Fig. S6 (in ESI), the introduction of the three additives increased the root-mean-square (RMS) roughness of both the PM6 and L8-BO neat films relative to that of the pristine films without additive treatment. AFM height images of the blend films are shown in Fig. 3(a). Comparing the additive-free film with a RMS roughness of 0.86 nm, the blend films processed with DFNB, DCNB, and DBNB exhibited increased RMS values of 1.26, 1.07, and 1.02 nm, respectively. The increased roughness could be attributed to enhanced molecular aggregation, as supported by the UV-Vis absorption spectra. TEM was employed to inspect the bulk morphology of the PM6:L8-BO blend films under different conditions. As shown in Fig. 3(b), the DCNB-treated PM6:L8-BO blend film exhibited a well-defined fibrillar network structure in contrast to the other three films. The interconnected fibrillar structure provided abundant D/A interfaces for exciton dissociation and continuous pathways for charge transport, thereby contributing to the enhanced J_{SC} and FF of the corresponding device.[6]

Grazing incidence wide-angle X-ray scattering (GIWAXS) was performed to investigate the effect of the three cyano-functionalized additives on the crystallinity of PM6:L8-BO blend films. The 2D-GIWAXS patterns and the corresponding scattering profiles of the blend films are shown in Figs. 4(a)–4(e), and the detailed parameters in the in-plane (IP) and out-of-plane (OOP) directions are summarized in Tables S8 and S9 (in ESI). All films exhibited a face-on dominant molecular packing orientation. Compared with the as-cast films, the blend films processed with the three additives exhibited enhanced scattering signals for both the (100) peaks in the IP direction and the (010) peaks in the OOP direction, indicating that the incorporation of additives effectively promoted more ordered molecular packing (Figs. 4a–4d). As depicted in Fig. 4(e), the DCNB- and DBNB-treated blend films exhibited notably sharper and more intense (100) diffraction peaks in the IP direction and (010) π–π stacking peaks in the OOP direction than the control and DFNB-treated films. In the IP direction, the DCNB- and DBNB-treated blend films showed substantially reduced FWHM values of 0.143 and 0.132 $Å^{-1}$ for the (100) peaks, respectively, compared with 0.179 and 0.170 $Å^{-1}$ for the control and DFNB-treated blend films, corresponding to increased CCLs of 40.823 and 44.221 Å versus 32.643 and 34.274 Å, respectively (Table S8 in ESI). Likewise, in the OOP direction, the DCNB- and DBNB-treated films exhibited re-

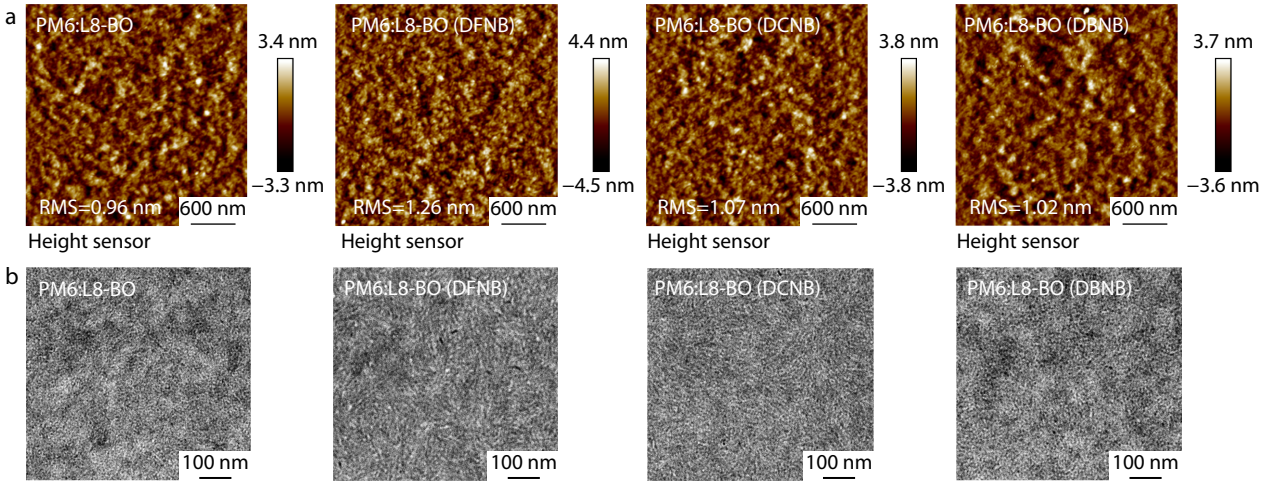


Fig. 3 (a) The AFM height images and (b) TEM images of PM6:L8-BO blend films with or without additives.

duced FWHM values and enhanced CCLs for the (010) peaks (Table S9 in ESI). Overall, these results demonstrate that the introduction of DCNB or DBNB promotes more ordered molecular packing and enhanced crystallinity of the PM6 donor and L8-BO acceptor in the blend films.

The long-term stability of OSCs is essential to assess their potential applications. To this end, we systematically compared the ambient storage stability of the best DCNB-treated devices with that of the control devices by tracking the evolution of their photovoltaic parameters throughout the aging process. As shown in Fig. 5(a), the DCNB-treated devices exhibited superior stability, retaining 87% of the initial PCE after 1900 h, versus 75% of that of the control devices. In addition, compared with the control devices, the DCNB-treated devices displayed significantly mitigated variations in V_{OC}, J_{SC}, and FF (Figs. 5b–5d), indicating that the introduction of DCNB effectively enhanced the long-term stability of the devices. Comparisons of the *J-V* curve evolutions are shown in Figs. 5(e) and 5(f).

To further verify the universality of DCNB, we employed the additive in PM6:Y6 and D18:L8-BO blend systems. As listed in Table S10 (in ESI), the corresponding DCNB-processed de-

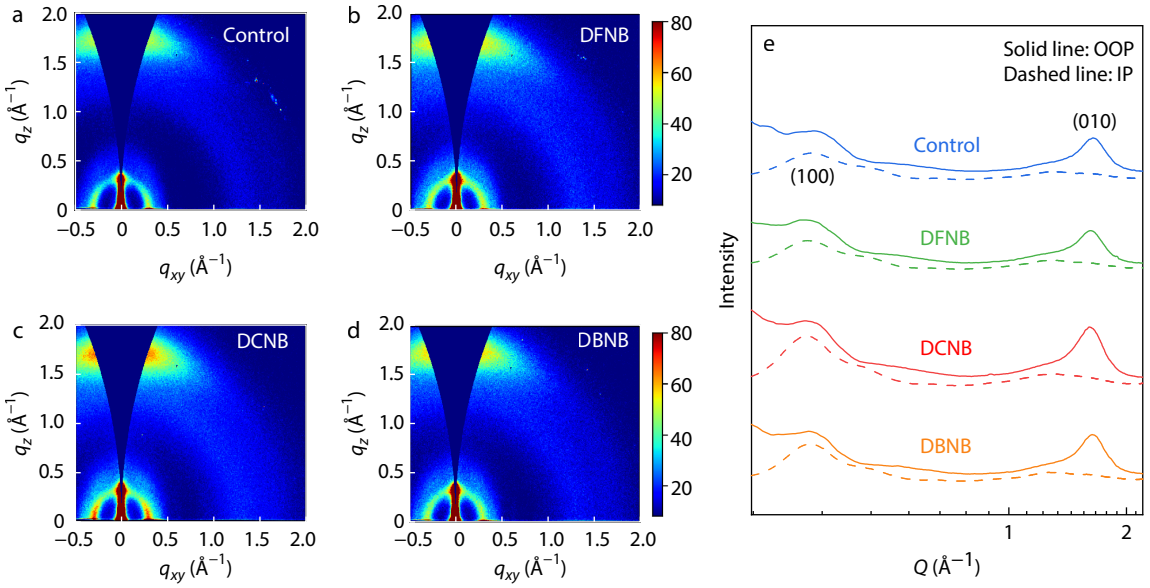


Fig. 4 (a–d) 2D-GIWAXS patterns and (e) the corresponding scattering profiles of PM6:L8-BO blend films with or without solid additives.

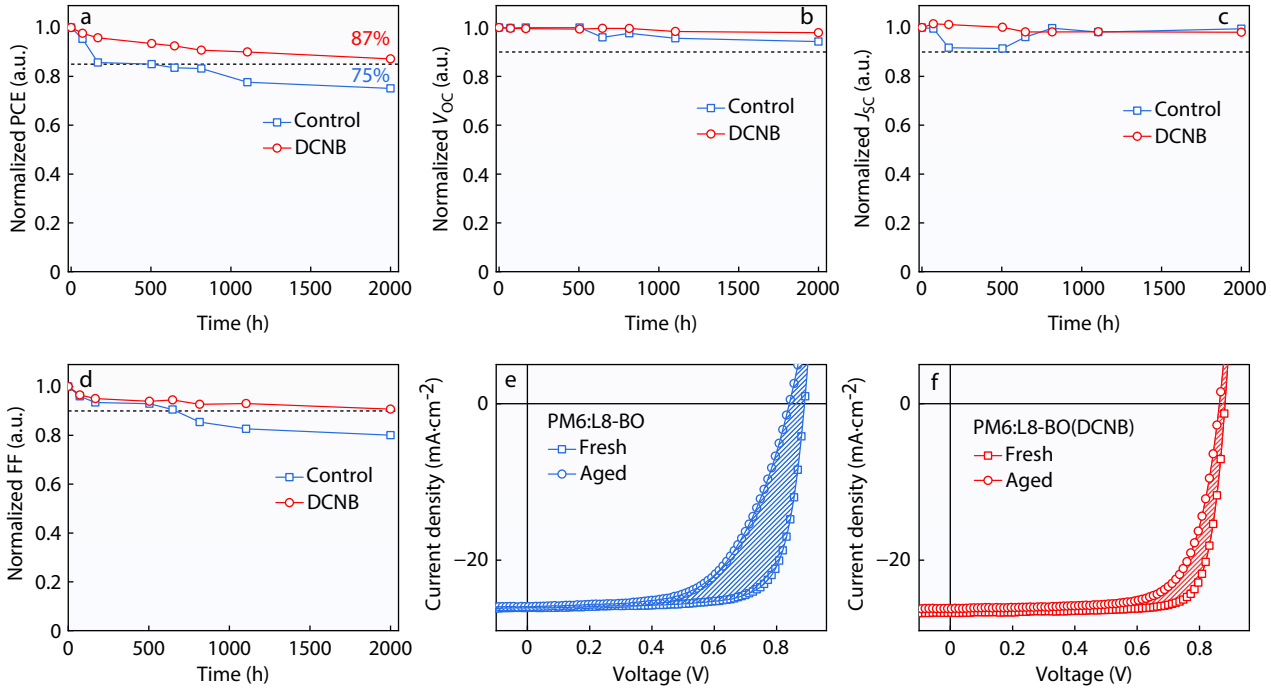


Fig. 5 Curves of the ambient storage stability: (a–d) time-dependent normalized PCE, V_{OC}, FF, and J_{SC} of DCNB-treated devices and the control devices. *J-V* curves of (e) the control devices, and (f) DCNB-treated devices before and after aging.

https://doi.org/10.1007/s10118-026-3869-1

vices delivered improved PCEs of 17.55% and 18.95%, respectively, compared to 16.95% and 18.24% for the relevant control devices.

CONCLUSIONS

Three volatile solid additives, DFNB, DCNB, and DBNB, were designed for the first time to optimize the morphology of PM6:L8-BO-based BHJ active layers. Theoretical simulations confirmed that all three additives exhibit significant intermolecular interactions with PM6 and L8-BO. These interactions enhance the aggregation of both the donor and acceptor, ultimately resulting in a fibrillar network. The introduction of these additives effectively suppressed bimolecular recombination while promoting exciton dissociation and charge transport, leading to remarkably improved photovoltaic performance of the OSCs. As a result, the DCNB-processed PM6:L8-BO devices achieved an outstanding PCE of 19.05% with superior ambient storage stability, retaining 87% of the initial PCE after 1900 h, versus 75% for the control devices. This study provides a novel strategy based on cyano-functionalized halogenated benzene additives for optimizing the morphology of efficient and stable OSCs.

Conflict of Interests

The authors declare no interest conflict.

Electronic Supplementary Information

Electronic supplementary information (ESI) is available free of charge in the online version of this article at http://doi.org/10.1007/s10118-026-3869-1.

Data Availability Statement

The data supporting the findings of this study are available from the corresponding author upon reasonable request.

ACKNOWLEDGMENTS

This work was financially supported by the National Natural Science Foundation of China (Nos. 52573195 and 22179040), National Key Research and Development Program of China (No. 2019YFA0705900), and the Basic and Applied Basic Research Major Program of Guangdong Province (No. 2019B030302007).

REFERENCES

1 Søndergaard, R.; Hösel, M.; Angmo, D.; Larsen-Olsen, T. T.; Krebs, F. C. Roll-to-roll fabrication of polymer solar cells. *Mater. Today* **2012**, *15*, 36–49.
2 Qin, F.; Wang, W.; Sun, L.; Jiang, X.; Hu, L.; Xiong, S.; Liu, T.; Dong, X.; Li, J.; Jiang, Y.; Hou, J.; Fukuda, K.; Someya, T.; Zhou, Y. Robust metal ion-chelated polymer interfacial layer for ultraflexible non-fullerene organic solar cells. *Nat. Commun.* **2020**, *11*, 4508.
3 Chatterjee, S.; Shimohara, N.; Seo, T.; Jinnai, S.; Moriyama, T.; Saida, M.; Omote, K.; Hama, K.; Iimuro, Y.; Watanabe, Y.; Ie, Y. Green-light wavelength-selective organic solar cells: module fabrication and crop evaluation towards agrivoltaics. *Mater. Today Energy* **2024**, *45*, 101673.
4 Song, J.; Zhang, C.; Li, C.; Qiao, J.; Yu, J.; Gao, J.; Wang, X.; Hao, X.; Tang, Z.; Lu, G.; Yang, R.; Yan, H.; Sun, Y. Non-halogenated solvent-processed organic solar cells with approaching 20 %

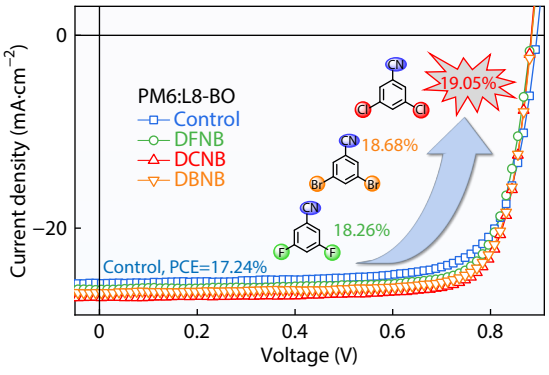
Graphical Abstract

Cyano-functionalized Halogenated Benzene Additives for Efficient and Stable Organic Solar Cells

Yang-Yang Zhang, Xiang-Lun Xie, Xin-Kang Wang, Kai-Yuan Lv, Tong-Jia Liu, Lian-Jie Zhang, and Jun-Wu Chen

South China University of Technology

The additive strategy plays a critical role in improving the performance of organic solar cells (OSCs). Herein, three highly volatile solid additives featuring a strongly electron-withdrawing cyano group 3,5-difluorobenzonitrile (DFNB), 3,5-dichlorobenzonitrile (DCNB), and 3,5-dibromobenzonitrile (DBNB) are introduced for the first time. Compared with the control device based on PM6:L8-BO (17.24%), devices processed with DFNB and DBNB exhibited enhanced power conversion efficiencies (PCEs) of 18.26% and 18.68%, respectively, whereas the DCNB-treated device achieved a champion PCE of 19.05%.



efficiency and improved photostability. *Angew. Chem. Int. Ed.* **2024**, *63*, e202404297.
5 Wupur, A.; Li, Y.; Luo, Y.; Chen, T.; Wang, M.; Zhang, Y.; Liu, Z.-X.; Wu, H.; Tan, H.; Zhang, Q.; Sun, X.; Hu, H.; Li, X.; Wu, J.; Fu, W.; Qiu, W.; Yang, X.; Chen, H. Unravel the distinctive roles of liquid and solid additives in blade-coated active layer for organic solar cell modules. *Adv. Energy Mater.* **2026**, *16*, 2403132.
6 Yang, X.; Xie, Y.; Tian, J.; Chen, J.; Zhang, Z.; Tang, D.; Shi, X.; Hao, X.; Zhang, J.; Ding, L.; Sun, Y.; Lv, M. Achieving a record fill factor of approaching 84% and 21% efficiency in binary organic solar cells *via* solid additive engineering. *Adv. Mater.* **2026**, *38*, e19230.
7 Li, D.; Kay, A. M.; Riley, D. B.; Sandberg, O. J.; Armin, A.; Meredith, P. Layer-by-layer processed pseudo-bilayer heterojunctions advance the performance of organic solar cells. *Adv. Energy Mater.* **2025**, *15*, 2500816.
8 Wang, J.; Wang, P.; Chen, T.; Zhao, W.; Wang, J.; Lan, B.; Feng, W.; Liu, H.; Liu, Y.; Wan, X.; Long, G.; Kan, B.; Chen, Y. Isomerism effect of 3D dimeric acceptors for non-halogenated solvent-processed organic solar cells with 20% efficiency. *Angew. Chem. Int. Ed.* **2025**, *64*, e202423562.
9 Jiang, Y.; Sun, S.; Xu, R.; Liu, F.; Miao, X.; Ran, G.; Liu, K.; Yi, Y.; Zhang, W.; Zhu, X. Non-fullerene acceptor with asymmetric structure and phenyl-substituted alkyl side chain for 20.2% efficiency organic solar cells. *Nat. Energy* **2024**, *9*, 975–986.
10 Heeger, A. J. 25th anniversary article: bulk heterojunction solar cells: understanding the mechanism of operation. *Adv. Mater.* **2014**, *26*, 10–28.
11 Kang, H.; Lee, W.; Oh, J.; Kim, T.; Lee, C.; Kim, B. J. From fullerene–polymer to all-polymer solar cells: the importance of molecular packing, orientation, and morphology control. *Acc. Chem. Res.* **2016**, *49*, 2424–2434.
12 Zhu, L.; Zhang, M.; Zhong, W.; Leng, S.; Zhou, G.; Zou, Y.; Su, X.; Ding, H.; Gu, P.; Liu, F.; Zhang, Y. Progress and prospects of the morphology of non-fullerene acceptor based high-efficiency organic solar cells. *Energy Environ. Sci.* **2021**, *14*, 4341–4357.
13 Yu, G.; Gao, J.; Hummelen, J. C.; Wudl, F.; Heeger, A. J. Polymer photovoltaic cells: enhanced efficiencies *via* a network of internal donor-acceptor heterojunctions. *Science* **1995**, *270*, 1789–1791.
14 Lee, H.; Park, C.; Sin, D. H.; Park, J. H.; Cho, K. Recent advances in morphology optimization for organic photovoltaics. *Adv. Mater.* **2018**, *30*, 1800453.
15 Xu, X.; Li, Y.; Peng, Q. Ternary blend organic solar cells: understanding the morphology from recent progress. *Adv. Mater.* **2022**, *34*, 2107476.
16 Li, X.; Huang, G.; Chen, W.; Jiang, H.; Qiao, S.; Yang, R. Size effect of two-dimensional conjugated space in photovoltaic polymers' side chain: balancing phase separation and charge transport. *ACS Appl. Mater. Interfaces* **2020**, *12*, 16670–16678.
17 Huang, Y.; Kramer, E. J.; Heeger, A. J.; Bazan, G. C. Bulk heterojunction solar cells: morphology and performance relationships. *Chem. Rev.* **2014**, *114*, 7006–7043.
18 Wu, L.; Wang, X.; Ng, M.; Song, Q.; Liu, S.; Ma, R.; Hu, L.; Xiong, L.; Xing, Z.; Li, Y.; Wu, J.; Zhang, M.; Liu, S.; Cai, Y. P.; Tang, M. C.; Liu, F.; Chen, J.; Li, G.; Jia, T.; Huang, F. A donor-acceptor integrated polymer for efficient organic solar cells. *Sci. Adv.* **2026**, *12*, eaec1922.
19 Yang, W.; Luo, Z.; Sun, R.; Guo, J.; Wang, T.; Wu, Y.; Wang, W.; Guo, J.; Wu, Q.; Shi, M.; Li, H.; Yang, C.; Min, J. Simultaneous enhanced efficiency and thermal stability in organic solar cells from a polymer acceptor additive. *Nat. Commun.* **2020**, *11*, 1218.
20 Al-Ibrahim, M.; Ambacher, O.; Sensfuss, S.; Gobsch, G. Effects of solvent and annealing on the improved performance of solar cells based on poly(3-hexylthiophene): fullerene. *Appl. Phys. Lett.* **2005**, *86*, 201120.
21 Sun, F.; Wu, J.; Cheng, B.; Kan, L.; Hua, F.; Sun, W.; Wang, H.; Huo, Y.; Chen, S.; Xia, X.; Du, X.; Liu, F.; Wang, E.; Guo, X.; Li, Y.; Zhang, M. Constructing continuous acceptor fibrillar networks and achieving uniform phase separation *via* polymer-assisted morphology control for 20.3% efficiency additive-free organic solar cells. *Energy Environ. Sci.* **2025**, *18*, 7071–7081.
22 Wei, Z.; Wang, Y.; Li, Y.; Gong, S.; Jiang, X.; Liu, Y.; Zhang, D.; Cho, Y.; Zhang, A.; Gao, L.; Cheng, Y.; Lu, H.; Li, H.; Liu, Y.; Yao, Y.; Zhang, C.; Liu, Q.; Cheng, P.; Facchetti, A.; Bo, Z.; Marks, T. J. High-efficiency, ultra-flexible organic solar cells enabled by chloroprene rubber as both a non-volatile solid additive and plasticizer. *Joule* **2025**, *9*, 101996.
23 Zhang, W.P.; Liu, M. M.; Fu, M. R.; Gao, D.; Zhao, Q. Q.; Xiao, B.; Zhao, T. X. "Bridging" structure polymer strategy for morphology regulation and performance optimization of organic solar cells based on the ternary-component polymer. *Chinese J. Polym. Sci.* **2026**, *44*, 813–820.
24 Wang, X.; Wu, J.; Zhao, S.; Chen, M.; Shi, T.; Xie, X.; Bai, Q.; Xie, J.; Zhang, L.; Ma, D.; Chen, J. Elevating dielectric constant *via* additive engineering: achieving 19.23% certified efficiency in thick-film binary organic solar cells. *Joule* **2025**, *9*, 102135.
25 Chen, K.; Duan, W.; Zhou, L.; Ma, R.; Li, P.; Zou, B.; Li, G. A systematic investigation on pyridine derived solid additives inducing fibrillar morphology for highly efficient organic solar cells with over 20 % efficiency. *Mater. Sci. Eng. R Rep.* **2025**, *164*, 100977.
26 McDowell, C.; Abdelsamie, M.; Toney, M. F.; Bazan, G. C. Solvent additives: key morphology-directing agents for solution-processed organic solar cells. *Adv. Mater.* **2018**, *30*, 1707114.
27 Fu, J.; Fong, P. W. K.; Liu, H.; Huang, C.-S.; Lu, X.; Lu, S.; Abdelsamie, M.; Kodalle, T.; Sutter-Fella, C. M.; Yang, Y.; Li, G. 19.31% binary organic solar cell and low non-radiative recombination enabled by non-monotonic intermediate state transition. *Nat. Commun.* **2023**, *14*, 1760.
28 Liu, B.; Gámez-Valenzuela, S.; Lee, J.-W.; Li, B.; Yang, W.; Wang, K.; Zhong, Z.; Yang, J.; Wang, Z.; Xu, C.; Sun, H.; Kim, B. J.; Guo, X. High-performance annealing-free polythiophene-based organic solar cells enabled by volatile solid additive. *ACS Energy Lett.* **2024**, *9*, 3727–3736.
29 Yu, R.; Yao, H.; Hong, L.; Qin, Y.; Zhu, J.; Cui, Y.; Li, S.; Hou, J. Design and application of volatilizable solid additives in non-fullerene organic solar cells. *Nat. Commun.* **2018**, *9*, 4645.
30 Song, X.; Zhang, K.; Guo, R.; Sun, K.; Zhou, Z.; Huang, S.; Huber, L.; Reus, M.; Zhou, J.; Schwartzkopf, M.; Roth, S. V.; Liu, W.; Liu, Y.; Zhu, W.; Müller-Buschbaum, P. Process-aid solid engineering triggers delicately modulation of Y-series non-fullerene acceptor for efficient organic solar cells. *Adv. Mater.* **2022**, *34*, 2200907.
31 Wang, J.; Wang, Y.; Bi, P.; Chen, Z.; Qiao, J.; Li, J.; Wang, W.; Zheng, Z.; Zhang, S.; Hao, X.; Hou, J. Binary organic solar cells with 19.2% efficiency enabled by solid additive. *Adv. Mater.* **2023**, *35*, 2301583.
32 Chen, J.; Zhang, L.; Jiang, X.; Gao, K.; Liu, F.; Gong, X.; Chen, J.; Cao, Y. Using *o*-chlorobenzaldehyde as a fast removable solvent additive during spin-coating PTB7-based active layers: high efficiency thick-film polymer solar cells. *Adv. Energy Mater.* **2017**, *7*, 1601344.
33 Kong, L.; Zhang, Z.; Zhao, N.; Cai, Z.; Zhang, J.; Luo, M.; Wang, X.; Chen, M.; Zhang, W.; Zhang, L.; Wei, Z.; Chen, J. *In situ* removable additive assisted organic solar cells achieving efficiency over 19% and fill factor exceeding 81%. *Adv. Energy Mater.* **2023**, *13*, 2300763.
34 Kong, L.; Wang, X.; Li, M.; Zhang, Z.; Chen, M.; Zhang, L.; Ying, L.; Ma, D.; Chen, J. *In-situ* removable solid additive optimizing active layer and cathode interlayer of organic solar cells. *Adv. Energy Mater.* **2024**, *14*, 2402517.
35 Zhang, Z.; Kong, L.; Wang, X.; Wang, R.; Tang, H.; Chen, M.; Yang,

Y.; Zhang, L.; Fu, Y.; Lu, X.; Ma, D.; Lüer, L.; Liu, C.; Brabec, C. J.; Chen, J. Cold-sublimating quasi-solid additive enables high efficiency and long operational stability binary organic solar cells. *Adv. Energy Mater.* **2026**, *16*, e05276.

36 Zhao, J.; Chung, S.; Li, H.; Zhao, Z.; Zhu, C.; Yin, J.; Cho, K.; Kan, Z. Impact of intermolecular interactions between halogenated volatile solid additives and the nonfullerene acceptor in organic solar cells. *Adv. Funct. Mater.* **2023**, *33*, 2307355.

37 Liu, H.; Bai, H.; Zhou, Y.; Li, P.; Su, W.; Liu, C.; Liao, X.; Song, B.; Li, X.; Bi, Z.; Zhao, C.; Liu, H.; Lu, G.; Du, H.; Jiang, L.; Liu, Y.; Ma, R.; Ma, W.; Fan, Q. Brominated isomerization engineering of 1-chloronaphthalene derived solid additives enables 19.68% efficiency organic solar cells. *Mater. Sci. Eng. R Rep.* **2025**, *162*, 100879.

38 Bannwarth, C.; Ehlert, S.; Grimme, S. $GFN_{2-x}TB$-an accurate and broadly parametrized self-consistent tight-binding quantum chemical method with multipole electrostatics and density-dependent dispersion contributions. *J. Chem. theory Comput.* **2019**, *15*, 1652−1671.

39 Chen, X.; Ren, C.; Chen, M.; Wang, X.; Yang, Y.; Xie, J.; Liu, L.; Zhang, L.; Ma, D.; Zhang, K.; Chen, J. Siloxane-tethered halogenated thiophene additives enable excellent fibrillar morphology and air processing for high-performing polymer solar cells. *Adv. Mater.* **2025**, *37*, e12197.

40 Mao, P.; Zhang, B.; Zhang, H.; Jiang, M.; Wang, Y.; Li, Y.; Wu, J.; Wang, J.-L.; An, Q. *In-situ* volatilization of solid additive assists as-cast organic solar cells with over 20% efficiency. *Mater. Sci. Eng. R Rep.* **2025**, *165*, 101022.

41 Cowan, S. R.; Roy, A.; Heeger, A. J. Recombination in polymer-fullerene bulk heterojunction solar cells. *Phys. Rev. B* **2010**, *82*, 245207.

42 Li, H.; Liu, L.; Yu, J.; Xie, J.; Bai, Y.; Yang, Z.; Dong, M.; Zhang, K.; Huang, F.; Cao, Y. High efficiency non-halogenated solvent processed organic solar cells through synergistic effects of layer-by-layer and solid additive. *Adv. Funct. Mater.* **2025**, *35*, 2505226.

43 Wen, L.; Mao, H.; Zhang, L.; Zhang, J.; Qin, Z.; Tan, L.; Chen, Y. Achieving desired pseudo-planar heterojunction organic solar cells *via* binary-dilution strategy. *Adv. Mater.* **2024**, *36*, 2308159.

44 Zhou, L.; Yu, H.; Zhang, J.; Qiu, D.; Fu, Y.; Yi, J.; Xie, L.; Li, X.; Meng, L.; Zhang, J.; Lu, X.; Wei, Z.; Li, Y.; Yan, H. Tailoring the position of ester group on *N*-alkyl chains of benzotriazole-based small molecule acceptors for high-performance organic solar cells. *Angew. Chem. Int. Ed.* **2024**, *136*, e202319635.